Strained bilayer WSe_2 with reduced exciton-phonon coupling

Ozgur Burak Aslan, [1] Minda Deng, [2, 3] Mark L. Brongersma, [1] Tony F. Heinz, [2, 3]

[1] Department of Materials Science and Engineering, and Geballe Laboratory for Advanced Materials, Stanford University, Stanford, California 94305, United States

[2] Department of Applied Physics, Stanford University, Stanford, California 94305, United States

[3] SLAC National Accelerator Laboratory, Menlo Park, California 94025, United States

Abstract

We investigate excitonic absorption and emission in bilayer WSe_2 under tensile strain. We observe a redshift of 110 meV in the energy of the A exciton absorption peak (at the direct gap at the K point in the Brillouin zone) under 2.1% uniaxial tensile strain. In addition, under the same strain, the spectral linewidth of the A exciton at room temperature decreases by a factor of two, from 70 to 36 meV. We show that this decrease is a result of suppression of phonon-mediated exciton scattering channels. This suppression is associated with the relative upshift under strain of the Q valley in the conduction band (involved in the indirect exciton emission), which is nearly degenerate with the K valley (involved in the A exciton). We analyze the strain-dependent absorption and photoluminescence spectra to determine the relative positions of these valleys and to infer intervalley scattering rates. Our model describes well the decrease and the distinct trends in the A exciton linewidth of monolayer and bilayer WSe_2 under strain. The results show that strain can be used to tune, as well as to probe, the relative energies of band extrema and exciton scattering channels in 2D semiconductors.

Introduction

Optical spectra of atomically thin semiconducting transition metal dichalcogenides (TMDCs) demonstrate dominant excitonic features due to their large excitonic binding energies and oscillator strengths [1-3]. It is thus crucial to understand the nature of excitons for fundamental studies on TMDCs and desirable to find approaches to tune them on demand for optoelectronic applications. In this respect, many recent studies have exploited strain to engineer the optical spectra of ultrathin TMDCs [4-12], exploiting these materials' unusually high in-plane mechanical strengths [13]. Significant changes to the optical absorption [12], redshifts exceeding 25% of the optical gap [4], indirect to direct gap transitions [6], and changes in the excitonic linewidths via strain have been reported in TMDCs [7,8,11,12,14,15]. In addition to the attractiveness of strain for altering the optoelectronic properties of these materials, the examination of such changes to the optical signatures provides insight into the many-body physics of excitons, the electronic band structure, and exciton-phonon scattering in TMDCs [12,14-17].

In this paper, we present investigations of the excitonic properties of bilayer (2L) TMDCs under strain, extending earlier studies for monolayer (1L) crystals [12,14,15]. The 2Ls present an interesting counterpart to the 1L materials. As is well known, the 2Ls possess indirect gaps, while the 1L materials generally have direct gaps. In both cases, however, the direct and indirect gaps lie only a few 10s to 100s of meV apart in energy [18-22]. Therefore, the exciton- and carrier-phonon scattering between the states associated with the direct and indirect gaps are expected to influence the optical and electrical properties of both 1Ls and 2Ls [21,23-25]. In fact, for the 1Ls, the consequences of using tensile strain in tuning the energy separation between states in different parts of the Brillouin zone and in significantly altering

scattering rates have been established [26-29]. Here we study whether and how related processes occur in the case of the indirect-gap 2L systems subjected to tensile strain, which has not yet been studied in the literature.

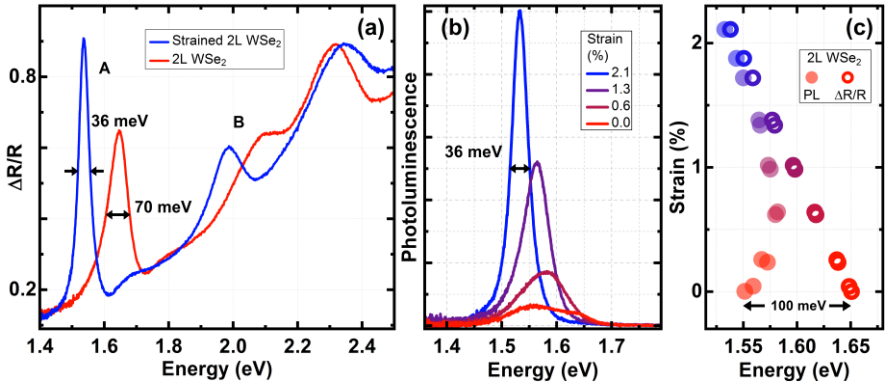


Figure 1: (a) Reflectance contrast spectra of 2.1% strained and unstrained 2L WSe_2. (b) Strain-dependent PL spectra of 2L WSe_2. (c) Strain dependence of the energy of the peak of PL and of absorption near the band edge of 2L WSe_2 (DOUBLE_COLUMN_FIGURE)

In particular, we examine the strain dependence of the linewidth of the lowest-lying direct exciton (KK or A exciton) in 2L WSe_2 and compare it to the previously reported behavior in 1L WSe_2 [12]. We observe a substantially different line narrowing in 2L WSe_2 from that seen in 1L WSe_2, despite the similar dependence of the material properties on strain. In 1L, the linewidth is most sensitive at small strain and decreases from 42 to 24 meV at 2.1% strain. However, in 2L the linewidth is nearly constant until a strain of 0.7% is reached, and the linewidth decreases more rapidly at larger strains in 2L than in 1L, decreasing from 70 to 36 meV. By making use of the experimentally determined strain dependence of the direct and indirect exciton energies, we calculate the strain-dependent intervalley scattering rate within the deformation potential approximation. We show that the decrease in the linewidth for 2L can be explained by a reduction of the phonon-mediated intervalley scattering rate from the direct to the lowest-lying indirect KQ (also known as $K\Lambda$) excitonic state as for the 1L. We then note that the different narrowing can be explained by the indirect nature of the gap in the unstrained 2L. Thus, we show that the model used on 1L WSe_2 and 1L WS_2 is applicable to 2L WSe_2 as well [12].

Experimental Methods

We mechanically exfoliate 2L WSe_2 from bulk crystals onto polydimethylsiloxane (PDMS) substrates [30]. After characterization of the samples by performing reflectance contrast and photoluminescence (PL) measurements, we transfer the 2L onto a 1.0 mm thick flexible polymer, polyethylene terephthalate glycol-modified (PETG). By bending the PETG substrate with a micromanipulator, we can incrementally apply uniaxial strain in a configuration compatible with reflectance contrast and PL studies. We exercise care to measure the reflectance and PL on the same sample location (within the spot size of the light beam) for a given strain level (see the Supplemental Material (SM) section S1 [31] for the related calculations of the strain).

[32-35]

Commented [BA1]: Cited only in SM

We obtain reflectance contrast spectra as $\Delta R/R = (R_{2L+PETG} - R_{PETG})/R_{PETG}$, where $R_{2L+PETG}$ and R_{PETG} are the reflectance of the 2L on the PETG substrate and of the bare PETG substrate [30]. These reflectance contrast spectra are approximately proportional to the absorption spectrum of the semiconductor layer [36]. For the reflectance

measurements, a tungsten-halogen lamp at a temperature of about 3400 K was focused down to a spot size of about 0.8 μm on the sample. For PL measurements, the 2Ls are excited with a 532-nm (2.33 eV) solid-state laser. A 40× objective with a numerical aperture (NA) of 0.6 was used for all measurements. The collected light was analyzed in a 300 mm focal length spectrometer equipped with a grating of 150 lines/mm. We obtained a spectral resolution of 0.8 meV around the peak energy of the A exciton.

We perform all sample fabrication and optical measurements at room temperature and without any other processing. This approach minimizes uncontrollable strain due to temperature changes. We note that the alignment of the crystallographic axes of the samples with respect to the direction of stain in our experiments is arbitrary. Within the regime of the strain we have examined in this study, we do not expect a significant dependence of the material properties on the direction of the axis of the strain relative to the crystallographic axes of the sample [37-39].

Results

---> Strain Dependence of the Optical Reflectance and Photoluminescence

We display the effect of strain on the reflectance contrast and PL of 2L WSe_2 in Figure 1. We analyze the strain-dependent reflectance spectra and extract the peak positions and the spectral linewidths of the excitons by fitting in a standard transfer matrix formalism [1,40]. As can be seen from the figure, the reflectance spectrum is dominated by the excitonic absorption peaks [3,36]. The peak amplitudes of the A and B exciton absorption features are observed to increase, while the corresponding linewidths can be seen to decrease under increasing strain. In particular, the linewidth $\gamma^{A\ exciton}$ of the A exciton absorption peak decreases from 70 to 36 meV for 2.1% strain. The oscillator strength of the A exciton absorption peak (proportional to the integrated area under the peak) is found to be nearly independent of strain (see SM section S2 for more reflectance spectra [31]). We note that the PL spectrum for the unstrained sample exhibits multiple peaks near the band edge, corresponding to the indirect and direct gaps. More strikingly, under 2.1% strain the linewidth of the PL feature decreases from about 142 meV for the unstrained sample to 36 meV, with the latter width matching that of the absorption feature under strain. This behavior is understood in terms of a strain-induced transition from an indirect to a direct gap material, as reported earlier by Desai *et al*. [6].

---> Energies of excitonic transitions under strain

We further analyze the spectra in Figure 1(a) and Figure 1(b) to gain more insight into the optical properties of 2L WSe_2. Figure 1(c) shows the strain-dependent energy of the A exciton extracted from the reflectance spectra, as well as the energy of the observed maximum of the feature in the PL spectra. The reflectance spectra show that the A exciton shifts from 1.65 eV to 1.54 eV and the B exciton shifts from 2.09 eV to 1.99 eV as the strain increases from 0.0% to 2.1%. We fit the PL spectrum under 0.0% strain to two Lorentzian line shapes and find that it exhibits multiple peaks around 1.55 eV and 1.64 eV. We see that the A exciton energy is 1.65 eV, while the PL spectrum exhibits a peak at 1.55 eV at 0.0% strain. We take the lower (higher) energy feature in the PL to reflect the energy of excitons for the indirect (direct) transition. As Figure 1(c) indicates, the energy of the maximum emission in the PL spectrum blueshifts until 0.7% strain is reached. However, the feature at the higher energy side, PL from the direct gap (KK), redshifts to 1.53 eV and dominates the PL spectrum at larger strain.

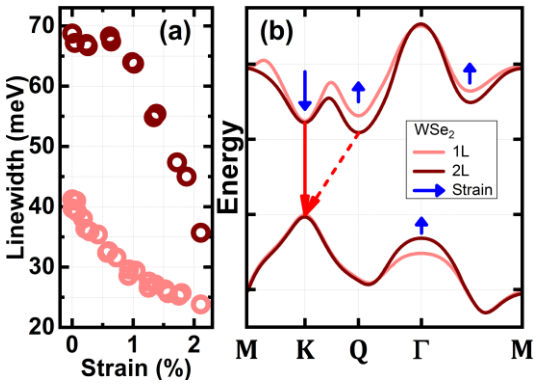


Figure 2: (a) Strain dependence of the linewidths of the A exciton in 1L and 2L WSe_2 (b) Schematic illustration of the valence and conduction bands of 1L and 2L WSe_2 (ignoring spin-orbit coupling) adapted from Ref. [41]. The solid red arrow indicates the direct gap transition (KK) of both 1L and 2L, whereas the dashed red arrow indicates the indirect gap transition (KQ) of 2L. Blue arrows indicate the direction and (qualitatively) the rate of the shift under strain of the selected extrema with respect to the K point maximum of the valence band [29,38].

---> Linewidths of excitonic transitions under strain

After having a better understanding of the strain-dependent exciton states of 2L and 1L WSe_2, we consider the influence of strain on the A exciton linewidth $\gamma^{A\,exciton}$. Figure 2(a) presents the results for 2L, as well as for 1L, WSe_2 [12]. We see that $\gamma^{A\,exciton}$ of 2L WSe_2 is about 70 meV at 0.0% strain and remains nearly unchanged for strains less than 0.7%. However, for larger strains, the linewidth decreases rapidly, at a rate >20 meV/% strain, reaching 36 meV at 2.1% strain. The trend suggests that the linewidth is likely to decrease still further at higher strains, which we did not examine experimentally. Despite the common overall trend of line narrowing under strain observed for 1L WSe_2, its behavior is quite different from that seen for the 2L samples: For the monolayer, $\gamma^{A\,exciton}$ already decreases at small strain and approaches a nearly constant asymptotic behavior at large strain [42]. Another observation is that although the unstrained 1L has a significantly smaller linewidth than the 2L, at 2.1% strain, linewidth (36 meV) of the 2L WSe_2 drops below that of the unstrained 1L WSe_2 (42 meV) [12].

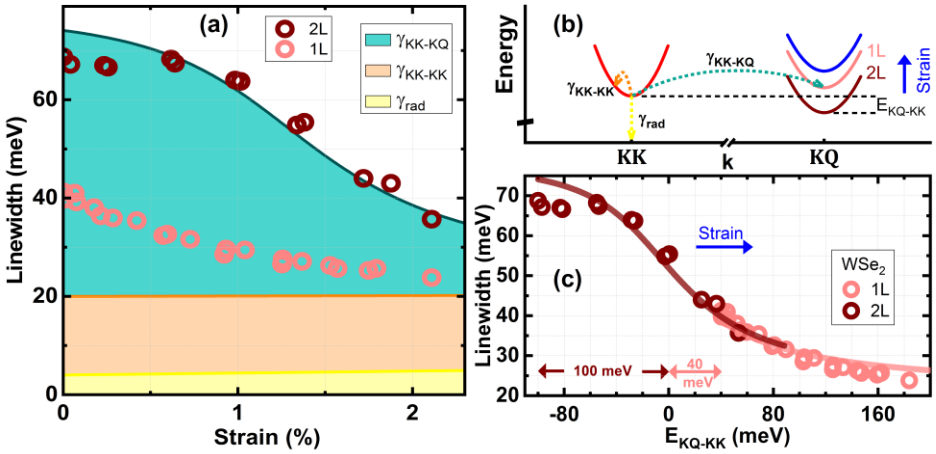


Figure 3: (a) Experimentally measured strain dependence of the linewidths of the A exciton in 1L and 2L WSe_2, and calculated contributions to the linewidth in 2L WSe_2. The heights of the colored areas between the solid lines represent, respectively, the contributions from the radiative decay γ_{rad} (yellow), intravalley exciton-phonon scattering γ_{KK-KK} (orange), and intervalley exciton-phonon scattering γ_{KK-KQ} (turquoise). (b) Schematic representation of the line broadening mechanisms and the strain dependence of the relative energy levels of KQ and KK states. (c) Linewidths of the A exciton in 1L and 2L WSe_2 as a function of calculated E_{KQ-KK} under strain. (DOUBLE_COLUMN_FIGURE)

Discussion

---> Indirect Gap of 2L: KQ or ΓK?

After confirming the indirect gap nature of the 2L, an important question to answer is whether the PL observed from the indirect gap (feature at 1.55eV at 0% strain in Figure 1(b)) is mediated via the KQ or ΓK transition [18]. To address this point, we inspect the valleys in the Brillouin zone of 2L WSe_2 and their behavior under strain. Let us note that we refer to the spin-allowed states with respect to the top of the K point in the valence band for the A exciton in this study, which are the higher and lower energy spin-states of the K and Q valleys in the conduction band, respectively [20]. Figure 2(b) depicts schematically the valence and conduction bands of 1L and 2L WSe_2. Blue arrows indicate the direction of the shift of the selected valley extrema with respect to the K point of the valence band under tensile strain. We first note that the KQ is the smallest indirect gap calculated for 2L WSe_2 [41]. Moreover, we see in Figure 1(b) that the feature of interest (at 1.55 eV at 0% strain) blueshifts with increasing strain, as opposed to the higher energy feature (at 1.65 eV at 0% strain). However, the ΓK transition is calculated to redshift under strain. Thus, we confirm that the lower energy feature in the PL we observe at 0.0%, corresponding to the indirect gap of 2L WSe_2, is a KQ transition. This conclusion is compatible with electronic structure calculations [6,41,43] as well as with micro-ARPES [44,45] and optical measurements under pressure and strain [6,46]. (We note that a differing conclusion was reached in [19].)

---> Effect of Strain on Line Broadening Mechanisms

Here we wish to discuss the noticeably different exciton linewidth $\gamma^{A\,exciton}$ and its strain dependence for 2L and 1L WSe_2. As has been established in previous investigations [12,14-17], the room-temperature exciton linewidth is strongly affected by exciton-phonon scattering. We expect that the change in this scattering rate with strain will be the dominant

contribution to the observed strain dependence of the linewidth. To examine the influence of exciton-phonon scattering more quantitatively, we implement the deformation potential model recently applied to the 1Ls of WSe_2 and WS_2 [12]. We assume that the carrier-phonon coupling matrix elements are the same for 2L and 1L WSe_2, as in the case of WS_2 investigated by Raja *et al.* [47]. We consider the three processes that primarily determine $\gamma^{A\ exciton}$ to be: Radiative decay (γ_{rad}), intravalley scattering (KK to KK exciton-phonon scattering; γ_{KK-KK}) and intervalley scattering (KK to KQ and KK to ΓK exciton-phonon scattering; γ_{KK-KQ} and $\gamma_{KK-\Gamma K}$, respectively) [24]. Despite the fact that the calculated ΓK state energy is closer to the KK state energy in the 2L than in the 1L [41], $\gamma_{KK-\Gamma K}$ is governed by a small deformation potential and we ignore this term [21]. KK to KK' intervalley scattering rate is negligible for 2L (akin to 1L) due to the relatively small deformation potentials of the associated scattering mechanisms [21,24] , as they require a spin-flip that is much slower than the other mechanisms considered [48]. We now consider these contributions for 2L and the effect of strain on them.

First, for the case of the radiative broadening γ_{rad} of the 2L, similar values have been measured for 1L and 2L WSe_2 [49,50], as expected from the nearly invariant oscillator strengths over layer thicknesses [3]. γ_{rad} is only a few meV [51-54], which is calculated to increase by about 10% per % strain for 1Ls [17]. We assume the same trend for 2L WSe_2. The effect of strain on γ_{rad} is plotted as the yellow area in Figure 3(a). Evidently, γ_{rad} is calculated to slightly increase, opposite to the overall trend [17,24,54].

Second, to analyze γ_{KK-KK}, we compare the properties of 2L to 1L and to apply the model for intravalley scattering [21]. We consider the strain-induced change in the KK exciton reduced mass (m_{KK}), mass density of the material, sound velocity and the related phonon frequencies [17,22,39]. Reports have shown that the effective hole masses at the K point in the valence band are essentially the same for 1L and 2L [45,55]. Calculations have yielded that the effective electron masses at the K point in the conduction band of the 2L are only negligibly greater than that of the 1L. Since the relevant phonon frequencies and the mass densities are essentially the same for 1L and 2L, we expect the same speed of sound as well [56]. Therefore, for simplicity, we assume that 1L and 2L WSe_2 have the same trend for γ_{KK-KK} under strain. Thus, we find that γ_{KK-KK} decreases by about 2% per % strain for 2L WSe_2 corresponding to a decrease of less than 1 meV at the largest strain achieved, plotted as the orange area in Figure 3(a) [16,24].

It is evident that the sum of γ_{KK-KK} and γ_{rad} (orange line in Figure 3(a)) is nearly constant under strain and they do not explain the significant reduction in the $\gamma^{A\ exciton}$ of the 2L observed under increasing strain. Further, unstrained 1L and 2L WSe_2 have appreciably different linewidths of 42 and 70 meV, respectively, which must also be accounted for.

We now turn to inspecting γ_{KK-KQ}, and its strain dependence. As is the case with γ_{KK-KK} and γ_{rad}, 1L and 2L have virtually the same material properties that influence γ_{KK-KQ}, with one important exception: The energy difference of the excitons, E_{KQ-KK}. Figure 3(b) schematically represents the line broadening mechanisms and the strain dependence of the relative energy levels of KQ and KK states for 1L and 2L WSe_2. We note that the 2L is an indirect gap material with a negative E_{KQ-KK}. To quantify E_{KQ-KK}, we turn to the PL spectra of the 2L in Figure 1(b) and note that $E_{KQ-KK} =$ -100 meV from Figure 1(c). As the PL from the KQ state of 1L is not readily determinable from experiment, we use our recent estimate of E_{KQ-KK} = 40 meV [12] which is consistent with ARPES measurements [45]. Thus, we expect a difference of 140 meV between the two materials for $E_{KQ-KK}(\varepsilon = 0)$. We note that the phonon energies of 1L and 2L WSe_2 are in the range of about 10 to 30 meV [21]. Thus, γ_{KK-KQ} in 2L is expected to have contributions from efficient scattering via phonon emission as well as phonon absorption. However, γ_{KK-KQ} in 1L is mediated via phonon absorption

only. Therefore, we infer that the significant linewidth difference of unstrained 1L and 2L WSe_2 stems primarily from having different values of E_{KQ-KK}. To interpret the behavior under strain, we realize that E_{KQ-KK} increases mainly due to weaker coupling between the orbitals contributing to the K point of the conduction band and stronger coupling between the orbitals contributing to the Q state of the conduction band under tensile strain [26-29,38]. As the E_{KQ-KK} increases, the density of available final states in the scattering process will decrease. Thus, γ_{KK-KQ} will decrease under tensile strain [21,26]. The schematic in Figure 3(b) exhibits this effect.

---> Effect of Strain on E_{KQ-KK}

To analyze the experimentally determined variation in A exciton linewidth with strain, we must first consider the strain dependence of E_{KQ-KK}, which, as we have just argued, will strongly influence the strain dependence of γ_{KK-KQ}. Writing the contributions to the exciton energy in terms of shifts of the band separation and shifts of the exciton binding energies under strain ε, we have

$$E_{KQ-KK}(\varepsilon) = E_{KQ}(\varepsilon) - E_{KK}(\varepsilon) = E_{KQ-KK}(0) + \Delta E_{KQ}^{quasiparticle}(\varepsilon) - \Delta E_{KQ}^{binding}(\varepsilon) - \Delta E_{KK}(\varepsilon) \quad (1)$$

Here $E_{KQ}(\varepsilon)$ and $E_{KK}(\varepsilon)$ are the strain-dependent energies of the KQ and KK excitons, respectively. $\Delta E_{KQ}^{quasiparticle}(\varepsilon)$, $\Delta E_{KQ}^{binding}(\varepsilon)$, and $\Delta E_{KK}(\varepsilon)$ are the changes induced by strain in the KQ quasiparticle gap, KQ exciton binding energy, and the KK exciton energy, respectively. We evaluate these quantities for 2L WSe_2 in the following manner: $\Delta E_{KK}(\varepsilon)$ = -52 meV/% strain is obtained directly from the experimental reflectance spectra presented above. $\Delta E_{KQ}^{binding}(\varepsilon)$ can be estimated from the change of the KQ exciton reduced mass with strain; we find $\Delta E_{KQ}^{binding}(\varepsilon)$ = -4 meV/% strain (see SM section S3 [31]). We extract $\Delta E_{KQ}^{quasiparticle}(\varepsilon)$ = 18 meV/% strain from density functional theory (DFT) calculations in the literature [6]. Combining these results, we obtain for the strain dependence of the relative energies of indirect and direct excitons

$$E_{KQ-KK}(\varepsilon) = -100\ meV + 74\ meV\frac{\varepsilon}{\%} \quad (2)$$

The enhancement of the PL with strain seen in Figure 1(b) is consistent with Equation (2): Increased E_{KQ-KK} at higher strain results in significantly more KK excitons in thermal equilibrium at room temperature, leading to stronger PL through the direct-gap emission channel. Equation (2) predicts an indirect to direct gap transition at $\varepsilon = 1.4\%$ when $E_{KQ-KK}(\varepsilon) = 0$ meV. In fact, Figure 1(c) shows that the peak positions in the band-edge absorption and emission spectra are close to one another for 1.4% strain, confirming this prediction. This value differs from the DFT calculations mainly due to a smaller calculated value for $E_{KQ-KK}(0)$ [6].

We infer that γ_{KK-KK} and γ_{rad} of the 2L contribute in total about 20 meV to the linewidth as in the 1L [12]. We account for them to deduce γ_{KK-KQ}. Our model fits the strain-dependent linewidth reasonably well, with γ_{KK-KQ} decreasing from 55 (21) meV to 17 (5) meV for 2L (1L) WSe_2, shown as the turquoise area in Figure 3(a). The trend of the 2L linewidth suggests a further decrease at larger strain due to suppression in the γ_{KK-KQ} with larger E_{KQ-KK}. Nevertheless, at such strain values, the band structure will be significantly affected and other scattering rates such as $\gamma_{KK-\Gamma K}$ may not be negligible anymore.

---> 1L vs 2L WSe_2

We have so far suggested that the distinct behavior under strain of $\gamma^{A\ exciton}$ of the 2L and 1L arises from their different KQ and KK gap separation under 0% strain, $E_{KQ-KK}(\varepsilon = 0)$. It is therefore useful to compare the dependence of linewidths on E_{KQ-KK} under strain. We plot the calculated and experimentally obtained $\gamma^{A\ exciton}$ values as a

function of E_{KQ-KK} in Figure 3(c). We recall that the other material properties that affect the linewidth are expected to change only weakly under strain. As a result, the calculated values for the two thicknesses match well in the range where the E_{KQ-KK} values overlap. The experimental values of the 2L on the side of large strain also match well the values of the 1L on the small strain side where the values of E_{KQ-KK} are comparable. This further verifies the essence of our conclusion that the dominant intrinsic material property giving rise to distinct $\gamma^{A\,exciton}$ for 1L and 2L WSe_2 is E_{KQ-KK}. This conclusion extends to the case of 1L WS_2 [12].

Here we elaborate on the distinct trends of $\gamma^{A\,exciton}$ of 1L and 2L WSe_2 under strain. $\gamma^{A\,exciton}$ of 2L is nearly unchanged for strains < 0.7%. This behavior reflects the fact that the contribution to γ_{KK-KQ} via phonon emission is not significantly affected until E_{KQ-KK} becomes comparable to the phonon energies, 10 to 30 meV [21]. Beyond that level of strain, $\gamma^{A\,exciton}$ starts decreasing rapidly, at a rate exceeding 20 meV/% strain, falling to 36 meV at 2.1% strain. The linewidth keeps decreasing with increasing strain until E_{KQ-KK} becomes positive and slightly larger than the phonon energies, at which point this scattering channel becomes and remains weak.

Figure 3(c) presents a picture that simultaneously explains the behavior of the 1L and 2L and the distinction between them. The larger measured reduction in linewidth in 2L WSe_2 (34 meV, 50% of the unstrained linewidth) than in 1L WSe_2 (18 meV, 40% of the unstrained linewidth) under the same strain applied reflects the different value of the exciton energies of the unstrained materials, $E_{KQ-KK}(0)$ (-100 meV vs 40 meV). Note that the change in E_{KQ-KK} with strain results in decreases of γ_{KK-KQ} that are proportionally much greater than the strain and are significantly different for 2L and 1L WSe_2.

---> Linewidth of the B Exciton

Figure 1(a) clearly shows that the linewidth of the B exciton is larger than that of the A exciton without strain. The state associated with the B exciton lies higher in energy, enabling relaxation channels beyond those presented above. One such relaxation channel is $\gamma_{KK-\Gamma K}$, which is not negligible for the B exciton as the energy difference between the same-spin KK and ΓK states is relatively small [41]. Nevertheless, we expect that the intervalley scattering rate γ_{KK-KQ} of the B exciton should also decrease with strain due to the relative shifts of the higher lying KK and KQ states. Experimentally, we do indeed observe a decrease in the B exciton linewidth of 2L WSe_2 (WS_2) at high strain as seen in Figure 1(a). However, a detailed and quantitative model to explain the linewidth narrowing observed the for B exciton with strain is more complicated and beyond the scope of this paper [57].

---> Influence of strain on other TMDC bilayers

In this study, we have focused our attention on 2L WSe_2 due to the small energy separation between the indirect (KQ) and direct (KK) gaps, E_{KQ-KK} [18,19]. Furthermore, as 2L is nearly indirect, PL from both gaps has been readily observed [6,58]. This enables directly determining E_{KQ-KK} of 2L WSe_2. Moreover, the small E_{KQ-KK} makes the optical spectra of the excitons sensitive to strain, yielding observable signatures. For instance, an indirect-to-direct gap transition has been observed in 2L WSe_2 [6]. However, in the case of the 2L MoS_2, $MoSe_2$, and WS_2, other scattering channels for the KK state are available due to the relatively higher-lying Γ valley in the valence band (such as the ΓK state forming an indirect gap) [59,60]. Those additional scattering channels make the effect of strain on the optical spectra more complicated [47] and may quench the PL from the KQ state, impeding the direct determination of E_{KQ-KK} [19]. Therefore, we present for completeness spectra from some of other 2L TMDCs (Figure 4), but have not attempted a quantitate analysis of the strain-dependent exciton energies of linewidths.

Figure 4 depicts the reflectance contrast spectra of 1L WS_2, 2L WS_2, 2L $MoSe_2$ and 2L $MoTe_2$ with and without tensile strain. [12] There are clear decreases in the linewidths of the peaks in these materials under strain. $\gamma^{A\,exciton}$ of 2L WS_2 decreases from 69 meV (better than typical [47]) to 41 meV; $\gamma^{A\,exciton}$ of 2L $MoSe_2$ decreases from 64 meV to 39 meV; $\gamma^{A\,exciton}$ of 2L $MoTe_2$ decreases from 79 meV to 57 meV at around 2.1% strain. We analyzed $\gamma^{A\,exciton}$ of 1L WS_2 in greater detail in our earlier study [12]. Our results suggest that such changes are strongly correlated to the influence of strain on the band structure and, thus exciton-phonon scattering.

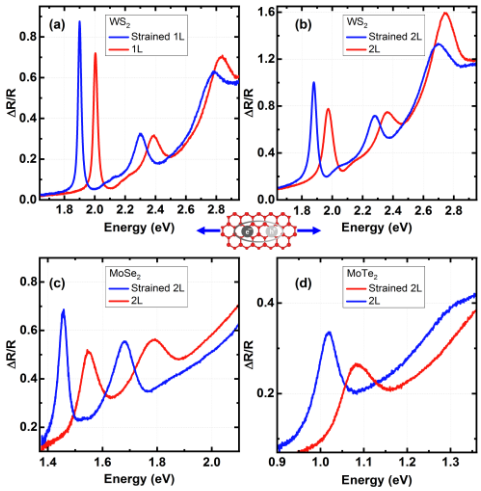


Figure 4: (a) Reflectance contrast spectrum of strained and unstrained (a) 1L WS_2, (b) 2L WS_2, (c) 2L $MoSe_2$, (d) 2L $MoTe_2$.

---> Does hBN Encapsulation Affect the Intrinsic Linewidth of 1L WSe_2?

Recent studies have reported the pronounced effect of hBN encapsulation on the exciton linewidths of 1L TMDCs [51,61]. There is clear evidence that hBN encapsulation provides a homogeneous dielectric environment for the excitons, resulting in significant reductions in their total linewidth [62], particularly at low temperatures. However, the different quantitative reductions on the linewidths of, for example, MoS_2 and WS_2 indicates that additional mechanisms may be playing a role [51]. Therefore, hBN encapsulation may be affecting the intrinsic linewidth of the excitons in ways that are different for different TMDCs. Interestingly, it is easy to observe a quantitative correlation between the effect of strain and hBN encapsulation on the exciton linewidths in TMDCs. For instance, the WSe_2 linewidth is most sensitive to strain and hBN encapsulation. To elaborate, given that the impact of strain on $\gamma^{A\,exciton}$ is mainly a result of the band structure changes, it is important to understand the effect of hBN on the band structure and other properties affecting the exciton-phonon scattering in TMDCs [14,51,63-65]. As our study showed, $\gamma^{A\,exciton}$ is less sensitive to the small changes to the band structure in the 2L than in 1L. This suggests that examining hBN encapsulated 1L and 2L WSe_2 samples may give a window into the importance of this effect. Furthermore, the same method will be helpful to study the effect of other atomically thin materials on one another. For instance, the effect of graphene on the band structures and the exciton linewidths of TMDCs can be investigated by comparing neighboring 1L and 2L WSe_2 samples under the dielectric influence of the same graphene sample [66,67].

Outlook

Our results suggest that compressive strain (excluding other factors such as wrinkle formation due to strain) may result in line broadening and PL quenching in 2D materials. Strain-dependent PL enhancement and linewidth can be

employed as a measure for strain imaging which will be useful for large scale growth of 2D materials [11]. Wafer-scale growth paves the way to flexible optoelectronics and our results will be beneficial to that field [68]. Strain-tuned interaction between the emission of 2D materials and the surrounding environment or other low dimensional materials can be studied. Heterostructures of strained 1Ls and other atomically thin materials will be useful for specific studies such as those in which the KQ state is desired to be far above the KK state. Thus, our study shows that strain engineering enables various studies and expands the limits of the 2D materials field.

Conclusion

In conclusion, we have performed optical spectroscopy on 2L WSe_2 under mechanical strain. Uniaxial tensile strain of 2.1% reduces its optical band gap by 110 meV to 1.54 eV. The energy of the maximum emission in the PL spectrum blueshifts for strains below 0.7% strain, but red shifts under higher strains. This non-monotonic behavior arises from the interplay of the indirect and direct gaps. We have shown that the indirect PL is a KQ transition in the Brillouin zone. Our calculations suggest that the WSe_2 bilayer changes from an optically indirect to a direct gap material at 1.4% strain. We have demonstrated that the exciton linewidths of 2L and 1L WSe_2, while both decreasing under increasing strain, show quite different behaviors. The difference stems from the indirect gap nature of the unstrained 2L. The line narrowing in the 2L is also a result of the increased energy separation between the lowest energy indirect and direct states, suppressing the phonon-induced intervalley scattering. $\gamma^{A\ exciton}$ becomes as small as 36 meV at 2.1% strain. Strained 2L WSe_2 is thus a material with an optical direct gap and reduced exciton-phonon coupling which can be viewed as an alternative to unstrained 1L WSe_2 for studies and applications that require a direct band gap material.

Acknowledgments

The experimental studies were supported by the MRSEC program of the National Science Foundation through Columbia University's Center for Precision Assembly of Superstratic and Superatomic Solids (Grant No. DMR-1420634). Spectroscopic analysis was supported by Department of Energy 'Photonics at Thermodynamic Limits' Energy Frontier Research Center under Grant No. DE-SC0019140 and modeling of the results was supported by the U.S. Air Force Office of Scientific Research (AFOSR) Multidisciplinary Research Program of the University Research Initiative (MURI) through Grant No. FA9550-17-1-0002.

Supplemental Material

Contents

S1 Applying Strain to PETG and WSe_2, and Its Calculation 11

S2 Strain-dependent Reflectance Spectra of 2L WSe_2 12

S3 Strain Dependence of the KK Quasiparticle Gap of 2L WSe_2 13

S4 Strain Dependence of the Binding Energy of the KQ and KK Excitons of 2L WSe_2 13

S1 Applying Strain to PETG and WSe_2, and Its Calculation

We apply strain to the polyethylene terephthalate glycol-modified (PETG) substrate, which has a rectangular cross section, in a symmetric 3-point bending geometry and calculate the strain from the vertical deflection at its center. The vertical deflection, z, is expressed in terms of the lateral distance from one of the end points of the substrate, x, the distance between the two support points, L, and the maximum deflection, which is at the center, z_{max}, as the following [32]:

$$z(x) = z_{max}\left(\frac{3x}{L} - \frac{4x^3}{L^3}\right) \text{for } 0 \le x \le \frac{L}{2}, \text{symmetric around } \frac{L}{2} \tag{3}$$

Next, we can obtain the radius of curvature of the substrate, R, along the axis connecting the two support points to calculate the strain, ε, as:

$$\varepsilon(x) = \frac{t}{2R} \tag{4}$$

We plot the results of Eq. (3) and Eq. (4) in Figure S1a and Figure S1a, respectively, for various specified strain values at the center of the substrate.

We place the PETG substrate such that the samples to be measured are at the center of the two support points. That way the strain calculations are more accurate and the optical measurements are easier specifically at large strain since the reflected light can be collected more efficiently.

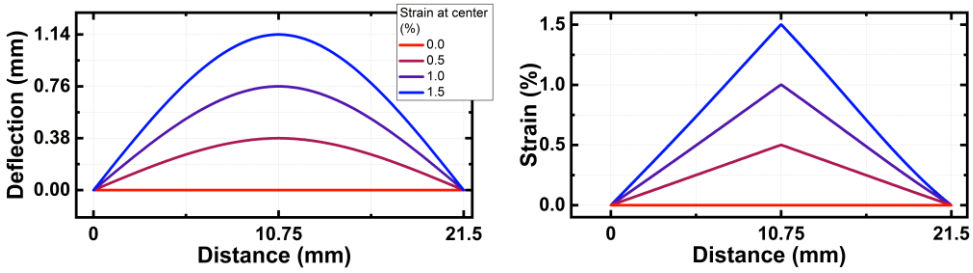


Figure S1: (a) Calculated deflection and strain as a function of the lateral distance over the PETG substrate from one of supporting points for various strain levels specified at the substrate center.

S2 Strain-dependent Reflectance Spectra of 2L WSe_2

Figure S2 plots the strain-dependent reflectance spectra of 2L WSe_2 ranging from 0.0% to 2.1% strain at various values. Figure S2a clearly shows that the features labeled, namely A_{1s} and B_{1s}, redshift with strain. We plot the same spectra by horizontally shifting them in Figure S2b such that the peak energies of the A_{1s} excitons match. The blueshift of the B_{1s} exciton relative to the A_{1s} exciton can be observed in Figure S2b. Such a blueshift is mainly attributed to the increased spin-splitting in the valence band [33,34].

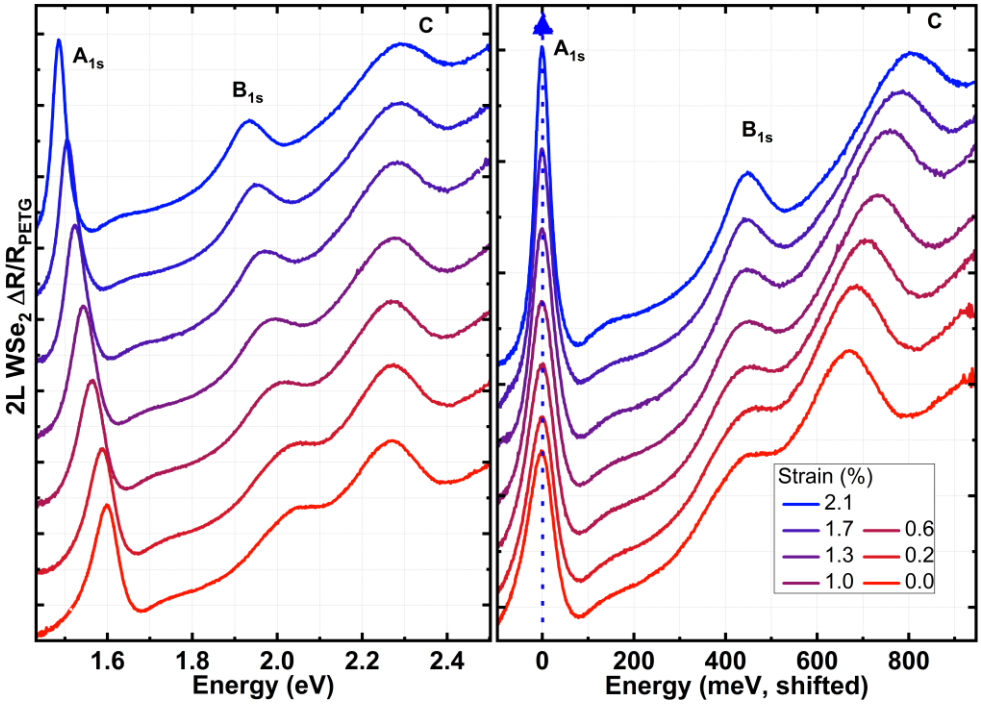


Figure S2: Strain-dependent reflectance contrast spectra of 2L WSe_2. Spectra are vertically offset for clarity in (a). Spectra are vertically offset as well as horizontally such that the peak energy of the A_{1s} exciton position relative to those of the other features observed can be emphasized in (b). The dashed line in (b) is a guide to the eye denoting the peak position of the A_{1s} exciton.

As mentioned in the main text, we analyze the strain-dependent reflectance spectra and extract the peak positions of the excitons by fitting in a standard transfer matrix formalism [1,40].

Since the PL spectra redshift with strain, we consider the energy-dependent collection efficiency of the optical elements. Those elements include the following: objective lens, mirrors, beam-splitting cube, long-pass filter, diffraction grating, Si CCD camera. Normalized collection efficiency is plotted in Figure S3. We see that the collection efficiency decreases by about 40% over the spectral range of the strain-dependent peak position of the A exciton. We correct the PL spectra accordingly. We stress that such a correction is crucial for accurately determining the strain dependence of PL intensity.

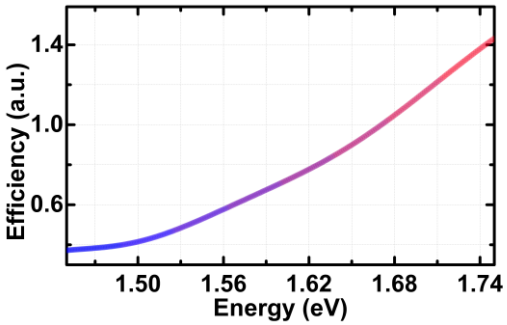


Figure S3: Collection efficiency of the optical path from the sample to the detector. The efficiency is normalized to be 1 at 1.67 eV, the peak energy of the A exciton PL of unstrained monolayer WSe_2.

S3 Strain Dependence of the Binding Energy of the KQ and KK Excitons of 2L WSe_2

Strain-dependent binding energy of the ground state KQ exciton, $\mathrm{E}_{KQ}^{binding}$, can be estimated by the strain dependence of its reduced mass, m_{KQ}, and comparing to those of the KK exciton of which the strain-dependent binding energy, $\mathrm{E}_{KK}^{binding}$, has been experimentally measured. Assuming that the excitonic binding energy is linearly proportional to the exciton reduced mass and assuming that applying strain does not cause significant changes the other factors that affect the binding energy, we write the following:

$$\mathrm{E}_{KQ}^{binding}(\varepsilon = 0) = \mathrm{E}_{KK}^{binding}(\varepsilon = 0)\frac{m_{KQ}}{m_{KK}}(\varepsilon = 0) \tag{5}$$

Then, we write the changes to the binding energies of KQ and KK excitons due to the changes in the exciton reduced masses as follows:

$$\begin{aligned}\Delta E_{KQ}^{binding}(\varepsilon) &= \mathrm{E}_{KQ}^{binding}(0)\frac{\Delta m_{KQ}(\varepsilon)}{m_{KQ}(0)} \\ \Delta E_{KK}^{binding}(\varepsilon) &= \mathrm{E}_{KK}^{binding}(0)\frac{\Delta m_{KK}(\varepsilon)}{m_{KK}(0)}\end{aligned} \tag{6}$$

Where m_{KQ} and m_{KK} are the reduced masses of the KQ and KK excitons, respectively. Substituting for $\mathrm{E}_{KQ}^{binding}(0)$ and $\mathrm{E}_{KK}^{binding}(0)$ yields the following:

$$\Delta E_{KQ}^{binding}(\varepsilon) = \Delta E_{KK}^{binding}(\varepsilon)\frac{\Delta m_{KQ}(\varepsilon)}{\Delta m_{KK}(\varepsilon)} \tag{7}$$

Now, we would like to obtain $E_{KK}^{binding}(\varepsilon)$ for 2L. However, the approach we followed for the 1L is not applicable to the 2L here as the excited states of the A exciton are not resolved in the optical spectra of the latter [12]. Thus, we first calculate $E_{KK}^{binding}$ for both 1L and 2L using the recently developed quantum electrostatic heterostructure model [35]. We obtain that $E_{KK}^{binding}$ is roughly 1.5 times larger for the 1L in accordance with the measurements on 1L and 2L WS_2 [1]. Thus, we obtain $E_{KK}^{binding}$ = -8 meV/% strain and $E_{KQ}^{binding}$ = -4 meV/% strain for 2L WSe_2.

S4 Strain Dependence of the KK Quasiparticle Gap of 2L WSe_2

Strain-induced change to the KK quasiparticle gap, $E_{KK}^{quasiparticle}$, can be expressed as:

$$\Delta E_{KK}^{quasiparticle}(\varepsilon) = \Delta E_{KK}(\varepsilon) + \Delta \mathrm{E}_{KK}^{binding}(\varepsilon) \tag{8}$$

$\Delta E_{KK}^{quasiparticle}(\varepsilon)$ and $\Delta E_{KK}^{binding}(\varepsilon)$ are changes induced by strain, ε, to KK quasiparticle gap and exciton binding energy, respectively.

For 2L WSe_2, we obtain $\Delta E_{KK}^{quasiparticle}(\varepsilon) =$ -60 meV/% strain, from the values reported in the paper ($\Delta E_{KK}(\varepsilon)$ = -52 meV/% strain, $\Delta E_{KK}^{binding}(\varepsilon)$ = -8 meV/% strain) , which matches the calculated value of -60 meV/% strain reported in Ref. [6].

References

[1] A. Chernikov, T. C. Berkelbach, H. M. Hill, A. Rigosi, Y. Li, O. B. Aslan, D. R. Reichman, M. S. Hybertsen, and T. F. Heinz, Phys. Rev. Lett. **113**, 076802 (2014).

[2] K. He, N. Kumar, L. Zhao, Z. Wang, K. F. Mak, H. Zhao, and J. Shan, Phys. Rev. Lett. **113**, 026803 (2014).

[3] Y. Li, A. Chernikov, X. Zhang, A. Rigosi, H. M. Hill, A. M. van der Zande, D. A. Chenet, E.-M. Shih, J. Hone, and T. F. Heinz, Phys. Rev. B **90**, 205422 (2014).

[4] D. Lloyd, X. H. Liu, J. W. Christopher, L. Cantley, A. Wadehra, B. L. Kim, B. B. Goldberg, A. K. Swan, and J. S. Bunch, Nano Lett. **16**, 5836 (2016).

[5] H. J. Conley, B. Wang, J. I. Ziegler, R. F. Haglund, S. T. Pantelides, and K. I. Bolotin, Nano Lett. **13**, 3626 (2013).

[6] S. B. Desai, G. Seol, J. S. Kang, H. Fang, C. Battaglia, R. Kapadia, J. W. Ager, J. Guo, and A. Javey, Nano Lett. **14**, 4592 (2014).

[7] R. Schmidt, I. Niehues, R. Schneider, M. Druppel, T. Deilmann, M. Rohlfing, S. M. de Vasconcellos, A. Castellanos-Gomez, and R. Bratschitsch, 2D Mater. **3**, 021011 (2016).

[8] J. T. Ji, A. M. Zhang, T. L. Xia, P. Gao, Y. H. Jie, Q. Zhang, and Q. M. Zhang, Chin. Phys. B **25**, 077802 (2016).

[9] K. He, C. Poole, K. F. Mak, and J. Shan, Nano Lett. **13**, 2931 (2013).

[10] J. O. Island, A. Kuc, E. H. Diependaal, R. Bratschitsch, H. S. J. van der Zant, T. Heine, and A. Castellanos-Gomez, Nanoscale **8**, 2589 (2016).

[11] G. H. Ahn, M. Amani, H. Rasool, D. H. Lien, J. P. Mastandrea, J. W. Ager, M. Dubey, D. C. Chrzan, A. M. Minor, and A. Javey, Nat. Commun. **8**, 608 (2017).

[12] O. B. Aslan, M. Deng, and T. F. Heinz, Phys. Rev. B **98**, 115308 (2018).

[13] S. Bertolazzi, J. Brivio, and A. Kis, ACS Nano **5**, 9703 (2011).

[14] I. Niehues, R. Schmidt, M. Druppel, P. Marauhn, D. Christiansen, M. Selig, G. Berghauser, D. Wigger, R. Schneider, L. Braasch, R. Koch, A. Castellanos-Gomez, T. Kuhn, A. Knorr, E. Malic, M. Rohlfing, S. Michaelis de Vasconcellos, and R. Bratschitsch, Nano Lett. **18**, 1751 (2018).

[15] O. B. Aslan, I. M. Datye, M. J. Mleczko, K. Sze Cheung, S. Krylyuk, A. Bruma, I. Kalish, A. V. Davydov, E. Pop, and T. F. Heinz, Nano Lett. **18**, 2485 (2018).

[16] Z. Khatibi, M. Feierabend, M. Selig, S. Brem, C. Linderalv, P. Erhart, and E. Malic, 2D Mater. **6**, 015015 (2019).

[17] M. Feierabend, A. Morlet, G. Berghauser, and E. Malic, Phys. Rev. B **96**, 045425 (2017).

[18] W. S. Yun, S. W. Han, S. C. Hong, I. G. Kim, and J. D. Lee, Phys. Rev. B **85**, 033305 (2012).

[19] W. J. Zhao, R. M. Ribeiro, M. L. Toh, A. Carvalho, C. Kloc, A. H. C. Neto, and G. Eda, Nano Lett. **13**, 5627 (2013).

[20] A. Kormanyos, G. Burkard, M. Gmitra, J. Fabian, V. Zolyomi, N. D. Drummond, and V. Fal'ko, 2D Mater. **2**, 022001 (2015).

[21] Z. H. Jin, X. D. Li, J. T. Mullen, and K. W. Kim, Phys. Rev. B **90**, 045422 (2014).

[22] M. Hosseini, M. Elahi, M. Pourfath, and D. Esseni, IEEE Trans. Electron Devices **62**, 3192 (2015).

[23] X. Li, J. T. Mullen, Z. Jin, K. M. Borysenko, M. Buongiorno Nardelli, and K. W. Kim, Phys. Rev. B **87**, 115418 (2013).

[24] M. Selig, G. Berghauser, A. Raja, P. Nagler, C. Schuller, T. F. Heinz, T. Korn, A. Chernikov, E. Malic, and A. Knorr, Nat. Commun. **7**, 13279 (2016).

[25] K. Kaasbjerg, K. S. Thygesen, and K. W. Jacobsen, Phys. Rev. B **85**, 115317 (2012).

[26] M. Hosseini, M. Elahi, M. Pourfath, and D. Esseni, Appl. Phys. Lett. **107**, 253503 (2015).

[27] C. E. P. Villegas and A. R. Rocha, J. Phys. Chem. C **119**, 11886 (2015).

[28] S. H. Rhim, Y. S. Kim, and A. J. Freeman, Appl. Phys. Lett. **107**, 241908 (2015).

[29] M. A. U. Absor, H. Kotaka, F. Ishii, and M. Saito, Phys. Rev. B **94**, 115131 (2016).
[30] O. B. Aslan, Ph.D. thesis, Columbia University, 2017.
[31]
[32] S. Timoshenko, *Strength of Materials* (Van Nostrand, New York, 1940).
[33] D. Le, A. Barinov, E. Preciado, M. Isarraraz, I. Tanabe, T. Komesu, C. Troha, L. Bartels, T. S. Rahman, and P. A. Dowben, J. Phys. Condens. Matter **27**, 182201 (2015).
[34] B. Amin, T. P. Kaloni, and U. Schwingenschlogl, RSC Adv. **4**, 34561 (2014).
[35] K. Andersen, S. Latini, and K. S. Thygesen, Nano Lett. **15**, 4616 (2015).
[36] Y. L. Li and T. F. Heinz, 2D Mater. **5**, 025021 (2018).
[37] C. R. Zhu, G. Wang, B. L. Liu, X. Marie, X. F. Qiao, X. Zhang, X. X. Wu, H. Fan, P. H. Tan, T. Amand, and B. Urbaszek, Phys. Rev. B **88**, 121301(R) (2013).
[38] C. H. Chang, X. F. Fan, S. H. Lin, and J. L. Kuo, Phys. Rev. B **88**, 195420 (2013).
[39] A. M. Dadgar, D. Scullion, K. Kang, D. Esposito, E.-H. Yang, I. P. Herman, M. A. Pimenta, E.-J. G. Santos, and A. N. Pasupathy, Chem. Mater. **30**, 5148 (2018).
[40] S. J. Byrnes, https://arxiv.org/abs/1603.02720v4 (2016).
[41] H. Sahin, S. Tongay, S. Horzum, W. Fan, J. Zhou, J. Li, J. Wu, and F. M. Peeters, Phys. Rev. B **87**, 165409 (2013).
[42] O. B. Aslan, Y. Yu, L. Cao, and M. Brongersma, (unpublished).
[43] T. Deilmann and K. S. Thygesen, 2D Mater. **6**, 035003 (2019).
[44] N. R. Wilson, P. V. Nguyen, K. Seyler, P. Rivera, A. J. Marsden, Z. P. L. Laker, G. C. Constantinescu, V. Kandyba, A. Barinov, N. D. M. Hine, X. D. Xu, and D. H. Cobden, Sci. Adv. **3**, e1601832 (2017).
[45] P. V. Nguyen, N. C. Teutsch, N. P. Wilson, J. Kahn, X. Xia, A. J. Graham, V. Kandyba, A. Giampietri, A. Barinov, G. C. Constantinescu, N. Yeung, N. D. M. Hine, X. Xu, D. H. Cobden, and N. R. Wilson, Nature **572**, 220 (2019).
[46] Y. X. Ye, X. M. Dou, K. Ding, D. S. Jiang, F. H. Yang, and B. Q. Sun, Nanoscale **8**, 10843 (2016).
[47] A. Raja, M. Selig, G. Berghauser, J. Yu, H. M. Hill, A. F. Rigosi, L. E. Brus, A. Knorr, T. F. Heinz, E. Malic, and A. Chernikov, Nano Lett. **18**, 6135 (2018).
[48] D. Christiansen, M. Selig, G. Berghauser, R. Schmidt, I. Niehues, R. Schneider, A. Arora, S. M. de Vasconcellos, R. Bratschitsch, E. Malic, and A. Knorr, Phys. Rev. Lett. **119**, 187402 (2017).
[49] C. Robert, D. Lagarde, F. Cadiz, G. Wang, B. Lassagne, T. Amand, A. Balocchi, P. Renucci, S. Tongay, B. Urbaszek, and X. Marie, Phys. Rev. B **93**, 205423 (2016).
[50] G. Wang, X. Marie, L. Bouet, M. Vidal, A. Balocchi, T. Amand, D. Lagarde, and B. Urbaszek, Appl. Phys. Lett. **105**, 182105 (2014).
[51] F. Cadiz, E. Courtade, C. Robert, G. Wang, Y. Shen, H. Cai, T. Taniguchi, K. Watanabe, H. Carrere, D. Lagarde, M. Manca, T. Amand, P. Renucci, S. Tongay, X. Marie, and B. Urbaszek, Phys. Rev. X **7**, 021026 (2017).
[52] C. Poellmann, P. Steinleitner, U. Leierseder, P. Nagler, G. Plechinger, M. Porer, R. Bratschitsch, C. Schuller, T. Korn, and R. Huber, Nat. Mater. **14**, 889 (2015).
[53] T. Jakubczyk, V. Delmonte, M. Koperski, K. Nogajewski, C. Faugeras, W. Langbein, M. Potemski, and J. Kasprzak, Nano Lett. **16**, 5333 (2016).
[54] G. Moody, C. K. Dass, K. Hao, C. H. Chen, L. J. Li, A. Singh, K. Tran, G. Clark, X. D. Xu, G. Berghauser, E. Malic, A. Knorr, and X. Q. Li, Nat. Commun. **6**, 8315 (2015).
[55] B. Fallahazad, H. C. P. Movva, K. Kim, S. Larentis, T. Taniguchi, K. Watanabe, S. K. Banerjee, and E. Tutuc, Phys. Rev. Lett. **116**, 086601 (2016).
[56] P. Tonndorf, R. Schmidt, P. Boettger, X. Zhang, J. Boerner, A. Liebig, M. Albrecht, C. Kloc, O. Gordan, D. R. T. Zahn, S. M. de Vasconcellos, and R. Bratschitsch, Opt. Express **21**, 4908 (2013).
[57] I. Bernal-Villamil, G. Berghauser, M. Selig, I. Niehues, R. Schmidt, R. Schneider, P. Tonndorf, P. Erhart, S. M. de Vasconcellos, R. Bratschitsch, A. Knorr, and E. Malic, 2D Mater. **5**, 025011 (2018).
[58] W. Zhao, Z. Ghorannevis, L. Chu, M. Toh, C. Kloc, P.-H. Tan, and G. Eda, ACS Nano **7**, 791 (2013).
[59] A. Kumar and P. K. Ahluwalia, Model. Simul. Mater. Sc. Eng. **21**, 065015 (2013).
[60] R. Roldan, J. A. Silva-Guillen, M. P. Lopez-Sancho, F. Guinea, E. Cappelluti, and P. Ordejon, Ann Phys-Leipzig **526**, 347 (2014).
[61] O. A. Ajayi, J. V. Ardelean, G. D. Shepard, J. Wang, A. Antony, T. Taniguchi, K. Watanabe, T. F. Heinz, S. Strauf, X. Y. Zhu, and J. C. Hone, 2D Mater. **4**, 031011 (2017).

[62] A. Raja, L. Waldecker, J. Zipfel, Y. Cho, S. Brem, J. D. Ziegler, M. Kulig, T. Taniguchi, K. Watanabe, E. Malic, T. F. Heinz, T. C. Berkelbach, and A. Chernikov, Nat. Nanotechnol. **14**, 832 (2019).
[63] Z. Y. Huang, C. Y. He, X. Qi, H. Yang, W. L. Liu, X. L. Wei, X. Y. Peng, and J. X. Zhong, J. Phys. D Appl. Phys. **47**, 075301 (2014).
[64] M. K. L. Man, S. Deckoff-Jones, A. Winchester, G. S. Shi, G. Gupta, A. D. Mohite, S. Kar, E. Kioupakis, S. Talapatra, and K. M. Dani, Sci. Rep. **6**, 20890 (2016).
[65] C. Yelgel, O. C. Yelgel, and O. Gulseren, J. Appl. Phys. **122**, 065303 (2017).
[66] A. Raja, A. Chaves, J. Yu, G. Arefe, H. M. Hill, A. F. Rigosi, T. C. Berkelbach, P. Nagler, C. Schuller, T. Korn, C. Nuckolls, J. Hone, L. E. Brus, T. F. Heinz, D. R. Reichman, and A. Chernikov, Nat. Commun. **8**, 15251 (2017).
[67] H. M. Hill, A. F. Rigosi, A. Raja, A. Chernikov, C. Roquelet, and T. F. Heinz, Phys. Rev. B **96**, 205401 (2017).
[68] K. Kang, S. E. Xie, L. J. Huang, Y. M. Han, P. Y. Huang, K. F. Mak, C. J. Kim, D. Muller, and J. Park, Nature **520**, 656 (2015).